Journal of Colloid and Interface Science 475 (2016) 17–25

Contents lists available at ScienceDirect

Journal of Colloid and Interface Science

journal homepage: www.elsevier.com/locate/jcis

Development of a nanosphere adsorbent for the removal of fluoride from water

Kaisheng Zhang [a,b], Shibiao Wu [a], Junyong He [a,b], Liang Chen [a,b], Xingguo Cai [a,b], Kai Chen [a,b], Yulian Li [a,b], Bai Sun [a], Dongyue Lin [a], Guqing Liu [c], Lingtao Kong [a,*], Jinhuai Liu [a]

[a] Nano-Materials and Environmental Detection Laboratory, Hefei Institute of Intelligent Machines, Chinese Academy of Sciences, Hefei, Anhui 230031, PR China
[b] Department of Chemistry, University of Science and Technology of China, Hefei, Anhui 230026, PR China
[c] Bureau of Cultivated Land Protection, Sheyang, Jiangsu 224300, PR China

GRAPHICAL ABSTRACT

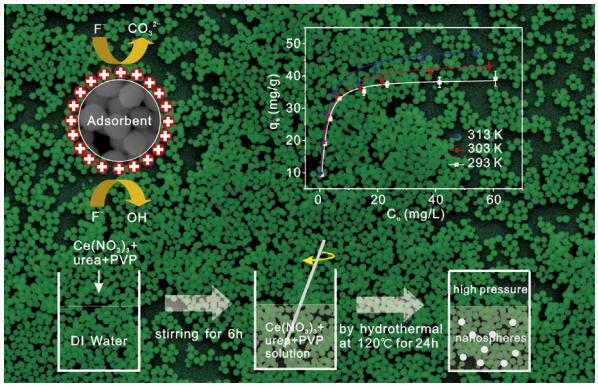

ARTICLE INFO

Article history:
Received 14 February 2016
Revised 15 April 2016
Accepted 22 April 2016
Available online 24 April 2016

Keywords:
$CeCO_3OH$ nanospheres
Fluoride
Adsorption
Carbonate

ABSTRACT

A new uniform-sized $CeCO_3OH$ nanosphere adsorbent was developed, and tested to establish its efficiency, using kinetic and thermodynamic studies, for fluoride removal. The results demonstrated that the $CeCO_3OH$ nanospheres exhibited much high adsorption capacities for fluoride anions due to electrostatic interactions and exchange of the carbonate and hydroxyl groups on the adsorbent surface with fluoride anions. Adsorption kinetics was fitted well by the pseudo-second-order model as compared to a pseudo-first-order rate expression, and adsorption isotherm data were well described by Langmuir model with max adsorption capacity of 45 mg/g at pH 7.0. Thermodynamic examination demonstrated that fluoride adsorption on the $CeCO_3OH$ nanospheres was reasonably endothermic and spontaneous. Moreover, the $CeCO_3OH$ nanospheres have less influence on adsorption of F^- by pH and co-exiting ions, such as SO_4^{2-}, Cl^-, HCO_3^-, CO_3^{2-}, NO_3^- and PO_4^{3-}, and the adsorption efficiency is very high at the low initial fluoride concentrations in the basis of the equilibrium adsorption capacities. This study indicated that the $CeCO_3OH$ nanospheres could be developed into a very viable technology for highly effective removal of fluoride from drinking water.

* Corresponding author.
E-mail address: ltkong@iim.ac.cn (L. Kong).

http://dx.doi.org/10.1016/j.jcis.2016.04.037
0021-9797/

1. Introduction

Fluoride can be present in drinking water, and it is considered beneficial at levels about 0.7 mg/L but hazardous if it exceeds 1.5 mg/L recommended by World Health Organization (WHO) [1]. Over the past decades, great efforts have been dedicated to searching for efficient alternative materials to improve their fluoride-adsorption capacity in water treatment [2]. Various materials, including layered double hydroxides [3,4], hydroxyapatite [5–7], activated alumina [8–10], zeolites [11,12] and ion-exchange resins [13,14], have been developed for the removal of fluoride. Among these materials, activated alumina is the most common adsorbent for defluoridation, but its disadvantages such as aluminum dissolution and relatively low adsorption capacity prevent it from wide application [15].

To increase the adsorption capacity of fluoride, rare earth, such as La, Ce or Zr, is usually used to prepare the efficient adsorbents, which is widely used in photocatalysis [16], catalysis [17], fuel cells [18], and especially the area of environmental management due to its special rare earth element properties [19]. For example, a novel Al-Ce hybrid adsorbent was prepared through the co-precipitation method. The defluoridation test demonstrated that high sorption capacity for fluoride was 27.5 mg/g at the equilibrium fluoride concentration of 1 mg/L for pH = 6 [20]. In addition, a granular Mn-Ce oxide adsorbent was prepared via co-precipitation method. Sorption isotherm showed that the sorption capacity of fluoride on the granular adsorbent were 45.5 mg/g at the equilibrium fluoride concentration of 1 mg/L for pH = 6 [21]. Besides, extensive research has been carried out in the design and preparation of nanostructures with different shapes and sizes because of their corresponding novel properties and potential applications for a few decades. CeO_2-ZrO_2 nanocages were prepared by Kirkendall effect, and their fluoride removal performance showed that the Langmuir maximum capacity reached to 175 mg/g and the optimum pH range was 3.5–4.5 [22]. Consequently, cerium compounds showed high removal capacities for fluoride due to its special properties, though these had narrow pH range. In general, anions are adsorbed on metal oxide based nanomaterials through electrostatic attraction and/or ion exchange. Surface hydroxyl groups are mainly reported to be involved in the ion exchange step. However, the synthesis of aluminium carbonate hydroxide nanospheres has been attempted, which had abundant carbonate groups on the surface area, and showed superb adsorption properties for AsO_4^{3-} and $Cr_2O_7^{2-}$ at pH 7, respectively [23]. This study confirmed a new adsorption mechanism involving ion exchange between carbonate groups and AsO_4^{3-} or $Cr_2O_7^{2-}$ species.

Apart from the above mentioned considerations, a one-step preparation without any following modification is regarded as an effective, energy-saving and labour-saving approach, in considering the direct formation of uniform-sized nanospheres during the synthesis process. However, one-step synthetic procedures for the synthesis of monodisperse $CeCO_3OH$ nanospheres are still a challenge because of the difficulty in manipulating the homogeneous nucleation and crystal growth. In this paper, we for the first time synthesized uniform-sized $CeCO_3OH$ nanospheres with a given amount of polyvinylpyrrolidone (PVP) by one-step hydrothermal procedure, which were characterized by SEM, XRD and XPS. Their defluoridation capacity and adsorption kinetics for fluoride were examined. The effects of pH, initial fluoride concentration and co-existing anions were investigated. The results show that the adsorbent possesses wide available pH range, high selectivity and excellent adsorption capacity for fluoride removal at the low initial fluoride concentrations. The fluoride removal mechanism indicated that the fluoride adsorption mainly resulted from the exchange of the carbonate and hydroxyl groups on the surface of the $CeCO_3OH$ nanospheres with fluoride anions and electrostatic interaction.

2. Experimental section

2.1. Synthetic details of the $CeCO_3OH$ nanospheres

All of the chemicals used for the synthesis of the $CeCO_3OH$ nanospheres were of analytical grade, which were received from Sinopharm Chemical Reagent Co., Ltd., Shanghai, China. Double distilled water was used throughout the experiment. The synthesis of the $CeCO_3OH$ nanospheres was based on a modified method of that investigated by Du et al. [24]. In a typical synthesis protocol, 2.5 mmol of $Ce(NO_3)_3{\cdot}6H_2O$, 37.5 mmol of urea and 12.6 μmol of PVP were dissolved in 90 mL deionized water with vigorous magnetic stirring at room temperature. The mixture was stirred continuously by using a magnetic stirrer for 6 h to form the transparent solution. And then the homogeneous solution was transferred into a 125 ml Teflon-lined stainless steel autoclave and maintained at 120 °C for 24 h. After the autoclave was cooled to room temperature naturally, the precipitates were collected by centrifugation and washed thoroughly with deionized water and ethanol for several times, and dried in an oven at 80 °C for 5 h. Thereafter the final products were characterized.

2.2. Materials characterizations

X-ray diffraction (XRD) patterns were obtained on an X'Pert-ProMPD diffractometer with Cu Ka radiation (λ = 0.15418 nm) at 40 kV and 200 mA. The scanning electron microscopy (SEM) images were taken by a field-emission scanning electron microscopy (FE-SEM, FEI Sirion 200 FEG, operated at 10 kV). For SEM characterization, 0.2 g $CeCO_3OH$ nanospheres were dispersed in 10 mL absolute ethyl alcohol, and then dripped onto the silica pellet and dried in the air for use. Thermo-gravimetric analysis (TGA) was tested on a SDT-Q600 DTG-TGA instrument by heating rate 10 °C/min in nitrogen flow. The nitrogen adsorption and desorption isotherms with a degassing temperature of 70 °C were carried out with a Micromeritics ASAP 2020 M + C analyzer. The Brunauer-Emmett-Teller (BET) specific surface and pore size distribution of adsorbent were tested by the nitrogen adsorption and desorption isotherms at 78 K. The adsorbent before and after fluoride adsorption was analyzed using X-ray photoelectron spectroscopy (XPS, VG ESCALAB MKII spectrometer, Mg K_α X-ray source, 1253.6 eV, 120 W) and Fourier transform infrared (transmission FT-IR, NEXUS-870 FT-IR spectrometer, KBr pellet) spectra in the range of 4000–400 cm^{-1}. The co-existing anions (bicarbonate, chloride, phosphate, nitrate and sulfate) concentration was measured by inductively coupled plasma atomic emission spectroscopy (ICP-AES). Surface charge measurements were performed on a Zeta Potential Analyzer (DelsaNano C/Z, Beckman, Coulter, USA, electromobility: -1.2×10^{-3} $cm^2/V\,s \sim +1.2 \times 10^{-3}$ $cm^2/V\,s$). Before measurement, 1 mg sample was diluted in 30 mL deionized water with different pH values and ultrasonicated for 3 min.

2.3. Fluoride adsorption

Fluoride anions (F^-) stock solution with a concentration of 1000 mg/L was prepared by dissolving 2.21 g sodium fluoride into 1000 mL deionized water. Fluoride-bearing solutions were obtained by diluting the stock solution to given concentrations with ultrapure water. The pH values were tested by pH electrode pH S-3C (Leici, China). The measurements of fluoride concentration were carried out using expandable ion analyzer with the fluoride

ion selective electrode PF-202-CF (Leici, China). Fluoride-bearing solutions were obtained by diluting the stock solution to given concentrations with ultrapure water and the calibration curve was calculated by the potential of the standard sodium fluoride solutions (0.1–60 mg/L) at pH = 5.0 (Fig. S1, see Supplementary material). The pH value was adjusted by using 0.1 mol/L HCl or NaOH.

The $CeCO_3OH$ nanospheres of 0.05 g was added into 50 mL fluoride-bearing solutions with the different initial fluoride concentrations (10, 20 and 30 mg/L, respectively). Kinetics experiments were conducted at 25 °C and pH = 7.0 in a shaker for 24 h. The mixtures were shaken at 150 rpm and approximately 5 mL aliquots were taken from the suspension at predetermined times. The residual adsorbent was quickly separated by centrifugation at 6000 rpm for 10 min and filtered with a 0.22 μm cellulose membrane and the corresponding residual fluoride concentration was measured by the fluoride ion selective electrode, in order to calculate their time-dependant adsorption capacities.

The adsorption isotherms were conducted with an adsorbent dose of 1 g/L at pH = 7.0 and 25 °C. Typically, 0.05 g adsorbent was added to 50 mL fluoride solutions of varying initial concentrations (10–100 mg/L). The solutions were oscillated at 150 rpm for 24 h with the constant stirring to achieve equilibrium. And then the residual adsorbent was separated by centrifugation and filtered with a 0.22 μm cellulose membrane. The residual fluoride concentration in solution was tested by the fluoride ion selective electrode. The defluoridation capacity at equilibrium of the adsorbents was calculated according to the following equation:

$$q_e = \frac{(C_0 - C_e)V}{m} \quad (1)$$

where C_0 and C_e represent the initial and equilibrium fluoride concentrations (mg/L) respectively, V is the volume of the fluoride solution (L), and m is the amount of the $CeCO_3OH$ nanospheres (g). The effect of pH and co-existing anions on the fluoride adsorption was studied at 25 °C for 24 h. The effect of pH on the fluoride adsorption was conducted using different initial fluoride concentrations (10, 20, and 30 mg/L, respectively), with 1 g/L of adsorbent and a total fluoride solution volume of 50 mL. The pH values were adjusted by using 0.1 mol/L HCl or NaOH solution. The effects of (bicarbonate, carbonate, nitrate, chloride, phosphate and sulfate) on fluoride adsorption were performed with an adsorbent dose of 1 g/L and an initial fluoride concentration of 10 mg/L at pH = 7.0. The co-existing anions were set at several concentration levels of 0, 0.25, 0.5, 1 and 2 mM, respectively. The mixed suspensions were shaken at 150 rpm. The method of testing the adsorption capability of the adsorbent was the same as the experiments above.

3. Results and discussion

3.1. Synthesis of the $CeCO_3OH$ nanospheres

When a given amount of PVP was introduced to the system, the size of the product could be nontrivially changed. From Fig. 1 the morphology of the as-prepared $CeCO_3OH$ nanospheres was observed by SEM, which is composed of many uniform nanospheres with an average diameter of 250 nm. High-magnification SEM image (inset in Fig. 1a) indicates that the surface of entire sphere is very smooth and size distribution (Fig. 1b) fits well with Gaussian distribution.

As we known, crystal growth at the nanoscale is an intricate process, governed by various factors, such as growth temperature, reactant pressure, monomer concentration, as well as surfactant [25]. To investigate the effect of the surfactant of PVP in the reactant solution on the morphology, samples were further synthesized by the same method but with different feeding amount of PVP in the reactant solution. Generally, the synthesis of the $CeCO_3OH$ nanospheres at the nanoscale is largely governed by the surfactant of PVP. When different feeding amount of PVP (0 mM, 0.06 mM, 0.14 mM, 0.22 mM, 0.28 mM, respectively) was introduced to the system, the morphology of the prepared products further investigated by SEM shown in Fig. S2, indicating that a given amount of PVP (0.14 mM) has played a pivotal role during the growth process of the $CeCO_3OH$ nanospheres. The synthesis method is simple and environmentally benign and the yield is nearly 100% based on the amounts of $Ce(NO_3)_3{\cdot}6H_2O$, and the method is quite easily scaled up to produce more than 20 g of the product in one batch using a big Teflon-lined stainless steel autoclave (Fig. S2f).

The crystal structure of the $CeCO_3OH$ nanospheres was examined by powder X-ray diffraction (XRD) shown in Fig. S3. As we can see, the product obtained from the hydrothermal method is single-phase. The diffraction peaks can be indexed to face-centered cubic phase Cerium Carbonate Hydroxide, $CeCO_3OH$ (JCPDS 041-0013) (Fig. S3).

To further study and quantify the pore structure of the $CeCO_3OH$ nanospheres, the nitrogen adsorption–desorption isotherms for adsorbent samples are shown in Fig. 2. The BET surface area and the pore volume of the as-prepared$CeCO_3OH$ nanospheres were 10.60 m^2/g and 0.041 cm^3/g, respectively.

The thermal stability of the $CeCO_3OH$ nanospheres was characterized by TG analysis, which was shown in Fig. 3. The TGA curve for the pyrolysis of as-prepared cerium carbonate hydrate was recorded in nitrogen atmosphere with a heating rate of 10 °C/min. The first weight loss at temperatures below 100 °C indicates the evaporation of H_2O. The drastic weight loss at temperatures from 220 to 450 °C is estimated to be 23.88 wt%, which is close to the theoretical weight loss (ca. 20.70 wt%) calculated on the following reaction.

$$4CeCO_3OH + O_2 \rightarrow 4CeO_2 + 4CO_2 + 2H_2O$$

Above 450 °C, $CeCO_3OH$ has been converted to CeO_2. Based on the above results, we concluded that the obtained samples are the $CeCO_3OH$ nanospheres, which was consist with result of XRD analysis. The results are confirmed by Du et al. [26], who concluded that a large weight loss is observed to start at 270 °C and finish at 500 °C and the total weight loss between 270 and 500 °C is measured to be about 23.80%, which is closed to the theoretical value calculated from the above reaction. Moreover, weight loss attributed to the burning of PVP was not detected, which means that PVP was almost completely removed by washing several times.

3.2. Fluoride adsorption property

The $CeCO_3OH$ nanospheres are tested for the adsorption of fluoride anions for water purification. In this study, the fluoride adsorption kinetic was conducted to investigate the adsorption rate, which governed the residence time of the adsorption reaction. Fig. 4 depicts the adsorption kinetics of fluoride on the $CeCO_3OH$ nanospheres at various initial concentrations with an adsorbent loading of 1 g/L at pH 7.0. It can be found that the adsorption happened rapidly in the first 3 h, more than 85% of fluoride could be removed, and then the adsorption capacity increased gradually until the adsorption equilibrium was achieved within 4 h. Therefore, an optimum shaking time of 4 h was chosen in the subsequent adsorption processes.

To further quantify the efficiency of fluoride adsorption with time, the kinetics processes were simulated by the pseudo-first-order and pseudo-second-order kinetic models. The pseudo-first-order model is expressed by the following equation, which is developed for irreversible adsorption of solid-water systems [27]:

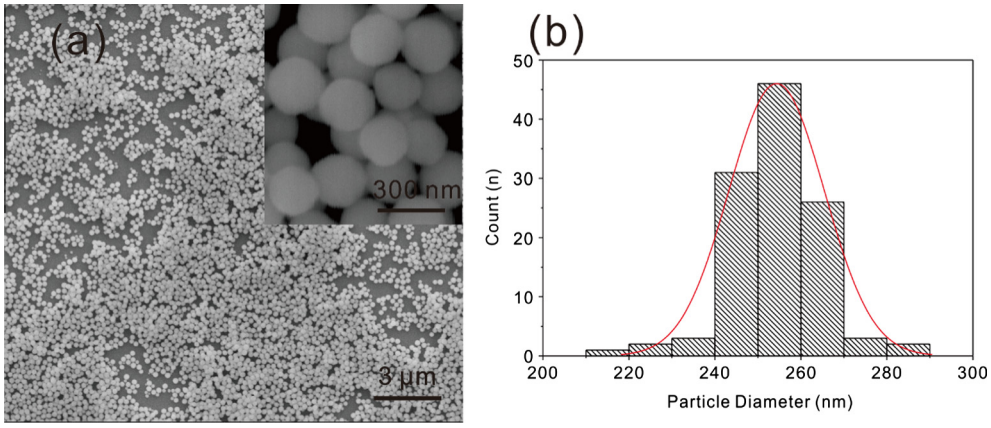

Fig. 1. (a) SEM (high-magnification SEM image inset) and (b) the corresponding size distribution of the $CeCO_3OH$ nanospheres, respectively.

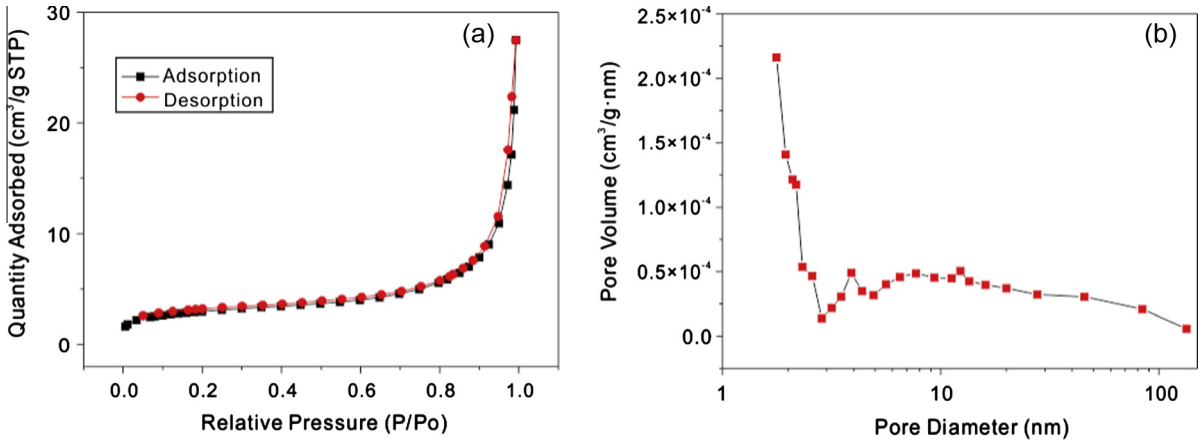

Fig. 2. N_2 adsorption/desorption isotherms and (b) pore size distributions of the as-prepared $CeCO_3OH$ nanospheres.

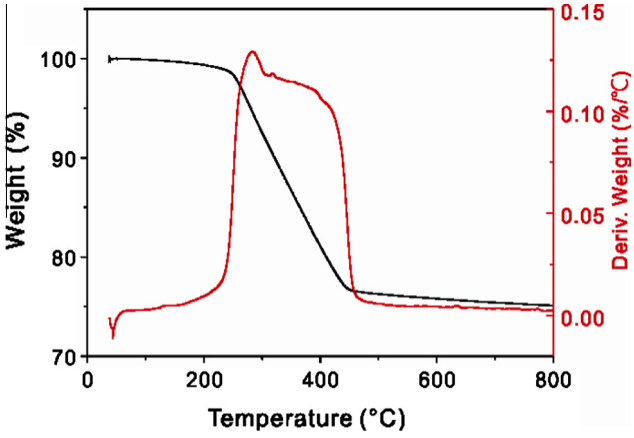

Fig. 3. The TGA curves of the as-prepared $CeCO_3OH$ nanospheres.

$$q_t = q_e(1 - e^{-k_1 t}) \quad (2)$$

where q_t and q_e are the amount of fluoride adsorbed (mg/g) at any time and at equilibrium, respectively. k_1 (min^{-1}) is the rate constant of the pseudo-first-order reaction. The pseudo-second-order model is described by following equation, which is based on the assumption that chemical adsorption is only one factor or one of the factors controlling the adsorption kinetics:

$$\frac{t}{q_t} = \frac{1}{k_2 q_e^2} + \frac{t}{q_e} \quad (3)$$

where q_t and q_e denote the amounts of fluoride adsorbed (mg/g) at any time and at equilibrium, respectively. k_2 is the rate constant for pseudo-second order reaction (g/(mg min)).

According to numerical simulation, the pseudo-second-order model fits better than pseudo-first-order model based on the values of determination coefficients (R^2) (Fig. S4). This suggested that the overall rate of the adsorption process was controlled by chemisorption which involved valency forces through sharing or exchange of electrons between the adsorbent and adsorbate [28]. Based on pseudo-second-order model, the equilibrium adsorption capacities ($q_{e,cal}$) were calculated as 9.78, 16.81, and 25.30 mg/g when the initial fluoride concentrations were 10, 20, and 30 mg/L, respectively, which were in agreement with the corresponding experimental values ($q_{e,exp}$) (Table 1).

To understand the performance of fluoride adsorption, adsorption isotherm of fluoride on the $CeCO_3OH$ nanospheres was shown in Fig. 5. The adsorption capacities increased with increasing fluoride concentrations. The experimental data was simulated with the Langmuir ($q_e = q_m \cdot k_L \cdot C_e/(C_e \cdot k_L + 1)$) and Freundlich ($q_e = k \cdot C_e^{1/n}$) models, respectively (Fig. 5 and Fig. S5) and the relative parameters calculated with the two models were listed in Table 2. Langmuir isotherm assumes monolayer adsorption onto a surface containing a finite number of adsorption sites of uniform strategies of adsorption with no transmigration of adsorbate in the plane of surface [29]. Freundlich model is an empirical equation

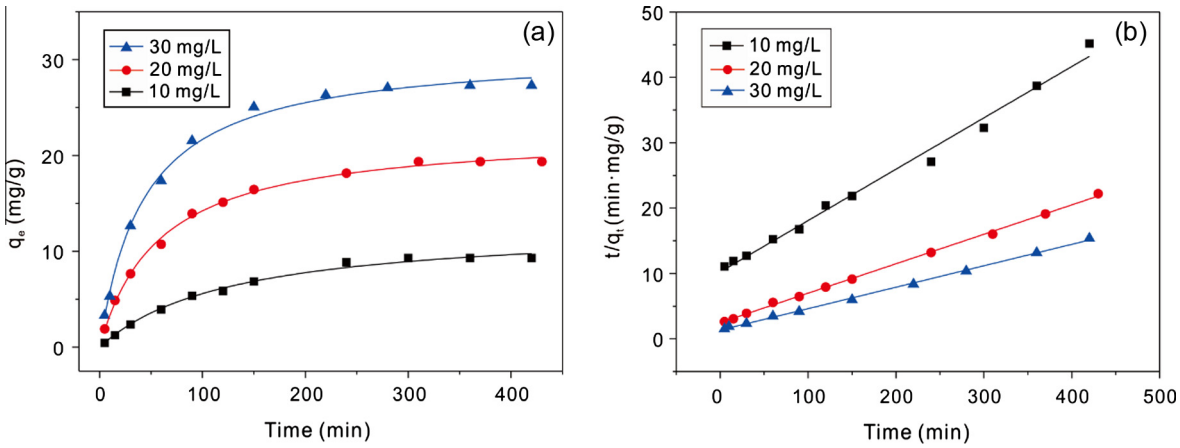

Fig. 4. (a) Kinetics of fluoride removal by the $CeCO_3OH$ nanospheres at different initial concentrations: 10 mg/L, 20 mg/L, 30 mg/L, respectively; (b) Pseudo–second–order kinetic plots of fluoride adsorption at different initial concentrations. (Adsorbent dose: 1 g/L, pH: 7.0 ± 0.2, temperature: 293 K).

Table 1
Kinetics parameters for fluoride adsorption on the $CeCO_3OH$ nanospheres with various initial fluoride concentrations.

Equations		Pseudo-first-order equation $\ln(q_e - q_t) = \ln q_e - k_1 t$			Pseudo-second-order equation $\frac{t}{q_t} = \frac{1}{k_2 q_e^2} + \frac{t}{q_e}$		
C_0 (mg/L)	$q_{e,exp}$ (mg/g)	k_1 (1/min)	$q_{e,cal}$ (mg/g)	R^2	k_2 [g/(mg·min)]	$q_{e,cal}$ (mg/g)	R^2
10	9.30	0.01196	9.78	0.941	6.02×10^{-4}	9.73	0.990
20	19.36	0.01134	16.81	0.993	8.17×10^{-4}	19.20	0.999
30	27.30	0.01589	25.30	0.994	8.06×10^{-4}	27.48	0.998

based on sorption on a heterogeneous surfaces or surfaces supporting sites of varied affinities. It is assumed that the stronger binding sites are occupied first and that the binding strength decreases with the increasing degree of site occupation [30]. According to the calculated results, the Langmuir model gave a better fit to the experimental data than Freundlich model with a determination coefficient value (R^2) of 0.999, which suggested that this process is monolayer adsorption onto the surface of adsorbent. The max adsorption capacities of fluoride could reach to 40.13, 43.73 and 48.15 mg/g at different temperatures, respectively. When equilibriums concentration was 1.5 mg/L (WHO guideline), the adsorption capacities of fluoride could be 17.36, 18.57, 20.89 mg/g, respectively. To the best of our knowledge, the as-prepared $CeCO_3OH$ nanospheres adsorbent achieved very good adsorption properties towards fluoride and they have much higher adsorption capacities than other defluoridation materials at equilibriums concentration of 1.5 mg/L (listed in Table 3). Besides, it could be found that the adsorption efficiency is very high at the low initial fluoride concentrations in the basis of the equilibrium adsorption capacities. For example, the fluoride removal ratio could reach up to 93.0%, 96.8% and 91.0% at room temperature and pH = 7 ± 0.2, when the initial fluoride concentration is 10 mg/L, 20 mg/L and 30 mg/L, respectively. Moreover, the thermodynamic parameters (ΔH°, ΔS°, and ΔG°) for fluoride adsorption on the$CeCO_3OH$ nanospheres can be calculated from the temperature-dependent adsorption isotherms (Figs. S5, S6 and Table S1 in Supplementary material).

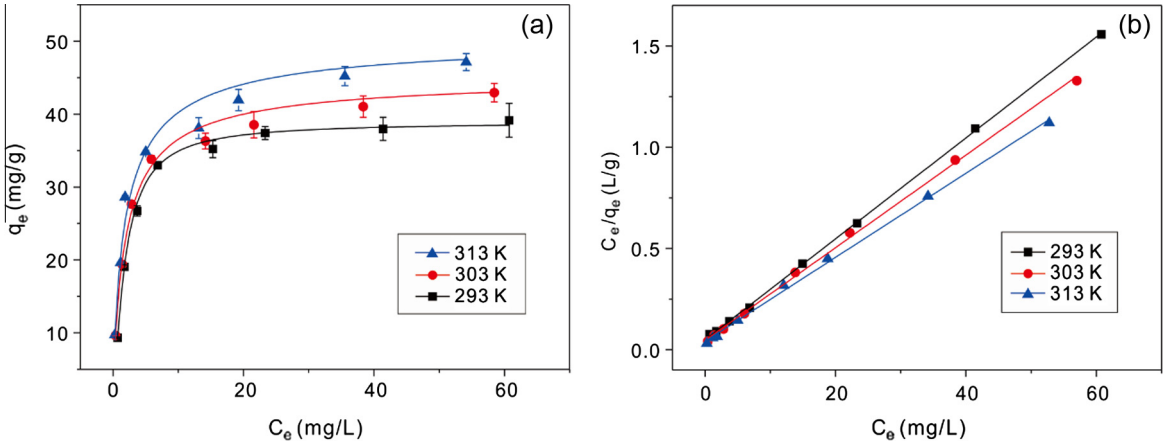

Fig. 5. (a) Adsorption isotherms of fluoride and (b) Langmuir isotherm models for fitting adsorption of fluoride by the $CeCO_3OH$ nanospheres at different temperatures (293 K, 303 K, 313 K, respectively) with adsorbent dose of 1 g/L at pH 7.0 ± 0.2.

Table 2
Langmuir and Freundlich adsorption isotherm parameters for fluoride adsorption by the $CeCO_3OH$ nanospheres.

Equations	Langmuir model $q_e = \frac{q_m k_L C_e}{1+k_L C_e}$			Freundlich model $q_e = kC_e^{1/n}$		
Temperature (K)	k_L (L/mg)	q_m(mg/g)	R^2	n	k	R^2
293	0.5083	40.13	0.999	3.496	14.77	0.786
303	0.4923	43.73	0.999	3.665	16.61	0.840
313	0.5111	48.15	0.998	3.677	18.18	0.848

Note: C_e is the equilibrium concentration of fluoride (mg/L); q_e is the amount of fluoride adsorbed on per weight of adsorbent after equilibrium (mg/g); q_m represents the maximum adsorption capacity of fluoride on per weight of adsorbent (mg/g); k_L is the Langmuir constant related to the energy of adsorption (L/mg). The Freundlich constant k is correlated to the relative adsorption capacity of the adsorbent (mg/g), and 1/n is the adsorption intensity.

Table 3
Comparison of adsorption capacity of some adsorbents for fluoride at equilibriums concentration of 1.5 mg/L.

Adsorbents	pH	Adsorption capacity (mg/g)	References
UiO-66(Zr)	6.8	8.60	[31]
CaO20@Al_2O_3	6.8	15.33	[32]
CeO_2/Mg–Fe layered double hydroxides	6–7	7.42	[33]
Cellulose@hydroxyapatite	N.A.	3.44	[5]
CeO_2–ZrO_2 nanocages	4	17.69	[22]
Hydrous ferric oxide doped alginate beads	7	1.93	[34]
Manganese oxide coated graphene oxide	6–7	1.13	[35]
Al (III) modified calcium hydroxyapatite	5	4.54	[36]
Granulated Fe–Al–Ce	7.0 ± 0.2	7.82	[37]
$CeCO_3OH$ nanospheres	7 ± 0.2	17.36	This work

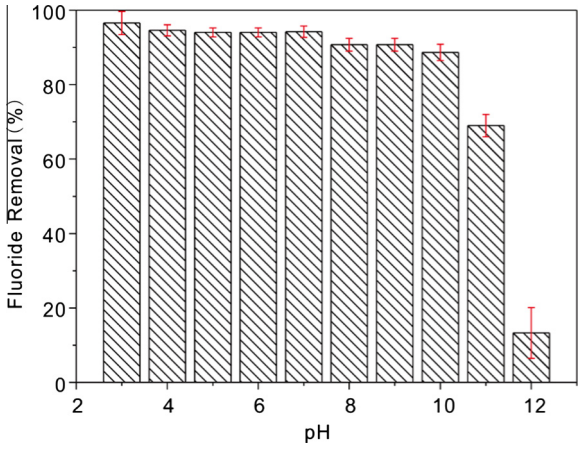

Fig. 6. Effect of pH on fluoride adsorption by the $CeCO_3OH$ nanospheres. Initial fluoride concentration: 10 mg/L, adsorbent dose: 1 g/L, temperature: 293 K.

The result indicates that the adsorption on the $CeCO_3OH$ nanospheres is an endothermic and spontaneous process.

The effect of the pH value for defluoridation by the $CeCO_3OH$ nanospheres with different initial pH values was investigated, as shown in Fig. 6. In this study, it is clear that the wide optimum pH values for the fluoride removal were at different pH ranging from 3 to 10 and the defluoridation capacities decreased with pH values increasing. To our knowledge, this is one of the widest pH ranges of today's materials for F^- adsorption. The maximum fluoride removal efficiency even reached up to 98% at pH 3 and the minimum one downed to 13% at pH 12 for initial fluoride concentrations of 10 mg/L. Such high removal ratio and wide alkaline pH range for fluoride adsorption are much better than that of any prior reports so far. The carbonate ions and hydroxyl groups exchanged with F^- are considered to be mainly responsible for the fluoride removal at the aqueous interface with the adsorbent. In most of the solid/liquid adsorption process, the solution pH has great effect in the adsorption capacity of the adsorbent due to the competition for the active sites by hydroxyl ions. However, exchange of the carbonate groups on the adsorbent surface could bring about wide pH range for fluoride removal, which was studied as the same as in our previous study [27].

Considering the complexity of water source, many anions might be present, such as SO_4^{2-}, Cl^-, HCO_3^-, CO_3^{2-}, NO_3^- and PO_4^{3-}. Thus, to reveal the effect of various co-existing anions upon adsorption of fluoride, these anions were added at different concentration levels (0, 0.25, 0.5, 1 and 2 mM, respectively) into fluoride solutions, and the fluoride removal efficiency was studied, as shown in Fig. 7. The results indicated that SO_4^{2-}, Cl^-, NO_3^- and PO_4^{3-} had little effect upon fluoride removal. The presence of HCO_3^- and CO_3^{2-} significantly affected the fluoride with the increase of their concentration. That is because HCO_3^- groups are hydrolyzed or ionized in solution, leading to the increase of pH value in the alkaline range and the increase of CO_3^{2-}concentrationsin the acidic pH range. As a result, more hydroxyl ions and CO_3^{2-} would compete with fluoride on the active adsorption sites, which resulted in the decrease of adsorption capacity of the $CeCO_3OH$ nanospheres for fluoride.

3.3. Adsorption mechanism

To further characterize the adsorption behavior of the obtained $CeCO_3OH$ nanospheres with F^-, Energy dispersive spectroscopy (EDS) analysis and EDS mapping before and after fluoride adsorption were performed and shown in Fig. 8 and S7. From Fig. 8, the strong peaks for the F^- were observed, indicating that F^- was effectively taken up by the adsorbent. Furthermore, the corresponding EDS mapping provides a direct elemental distribution on the surfaces of $CeCO_3OH$ nanospheres, and demonstrates that the $CeCO_3OH$ nanospheres are composed of Ce, O and C. EDS mapping further confirm that the F^- are uniformly adsorbed on the surface of the microsphere, which corresponds to result of the following FTIR and XPS analysis. In addition, the nanoparticles were not destroyed according to SEM images (Fig. 8a) after fluoride adsorption.

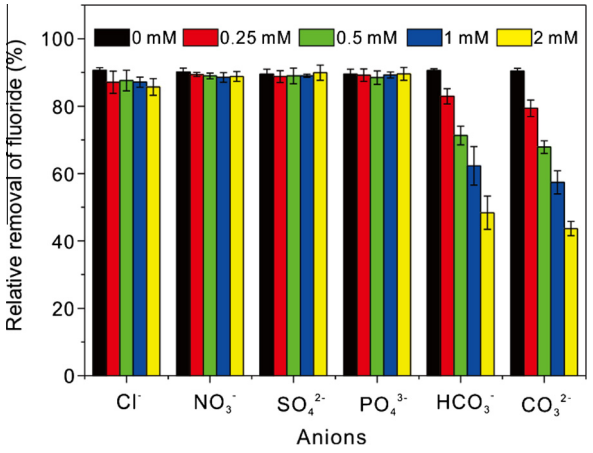

Fig. 7. Effects of co-existing anions on fluoride removal at fixed initial fluoride concentration of 10 mg/L. Adsorbent dose: 1 g/L, pH: 7.0 ± 0.2, temperature: 293 K.

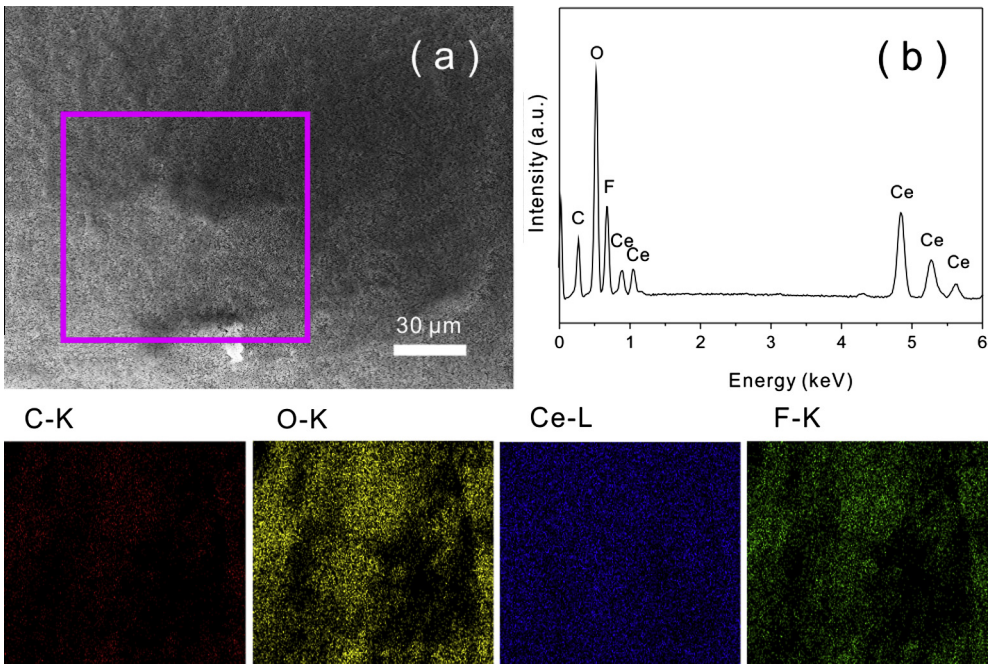

Fig. 8. (a) SEM image of the obtained $CeCO_3OH$ nanospheres after F^- adsorption; (b) EDS of the plotted area and EDS mapping of C, O, Ce and F for the $CeCO_3OH$ nanospheres after adsorption of F^-.

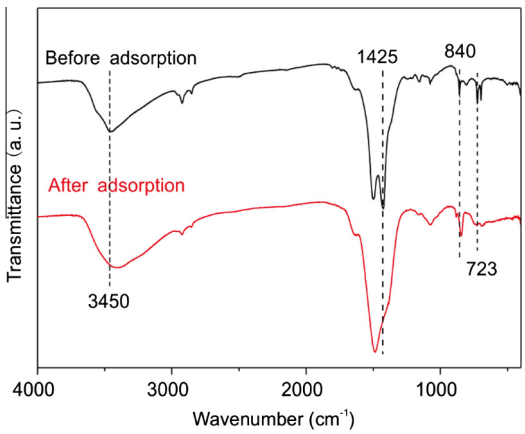

Fig. 9. FTIR spectra of the obtained $CeCO_3OH$ nanospheres before and after fluoride adsorption.

The FT-IR spectra of the $CeCO_3OH$ nanospheres before and after fluoride adsorption are shown in Fig. 9. The strong FT-IR peak at 1425 cm^{-1} is assigned to C-O stretching vibration of carbonate groups, the sharp peaks at 723 and 840 cm^{-1} are due to carbonate groups bending vibration, and the peak at 3450 cm^{-1} is due to —OH groups, as reported in other works [38–40]. Peaks at 2800–2900 cm^{-1} can be ascribed to the stretching bonds of C—H groups, which come from the adsorbed ethanol. These results are similar to Zhai's research [41], which concluded that the peaks at 1490 and 1410 cm^{-1} are assigned to the bending vibration of C—H bands and O—C—O stretching of the surfactant, and the peaks at 1070, 840, 723 cm^{-1} are attributed to νC—O, δCO_3^{2-} and $V_{as}CO_2$, respectively. After fluoride removal, the peaks at 723, 840 and 1425 cm^{-1}, turn very weak indicating carbonate groups partly lost, which verified the important roles of carbonate groups in the adsorption of fluoride. Moreover, the peak of 3450 cm^{-1} became weak after fluoride adsorption, thus, we can conclude that carbonate and hydroxyl groups exchanged with fluoride ions was involved in the adsorption of fluoride.

To further reveal the fluoride adsorption mechanism, the $CeCO_3OH$ nanospheres before and after fluoride adsorption were characterized by XPS. From the survey spectra shown in Fig. 10a, it is clear that the peak located at 684 eV was detected after fluoride adsorption. This was further confirmed by the F1s spectrum, as shown in Fig. 10b. The results suggested that the fluoride was successfully absorbed by the $CeCO_3OH$ nanospheres adsorbent. Quantitative analysis shows the fluoride molar ratio in the $CeCO_3OH$ nanospheres is 14.98% after adsorption. Fig. 10c and d presents the O1s spectra before and after fluoride adsorption, respectively. O1s spectra of the $CeCO_3OH$ nanospheres before fluoride adsorption suggests that three peaks located at 530.8, 531.7 and 532.4 eV can be are assigned to surface hydroxyl, carbonate groups and adsorbed water, respectively [22,42]. The surface hydroxyl and carbonate groups, which were proven to be the key factor for fluoride adsorption, occupied 87.39% in the $CeCO_3OH$ nanospheres. After fluoride adsorption, the content of the surface hydroxyl groups decreased from 34.37% to 33.01%, and carbonate groups decreased from 53.02 to 51.02%. The results further confirm an important role of the surface hydroxyl groups and carbonate groups in the adsorption of fluoride, which is consistent with the result of FT-IR analysis.

In addition, the zeta potential of the $CeCO_3OH$ nanospheres at different pH was depicted in Fig. 11, it can be found that the values of zeta potential decrease with the increase of pH. When the pH value is less than 10, the $CeCO_3OH$ nanospheres are positively charged, resulting in the improvement of fluoride removal. When the pH value is 6–10, the values of Zeta potential became stable, the fluoride removal is stabilized. When the pH value is more than 10, the $CeCO_3OH$ nanospheres are negatively charged, resulting in the reduction of fluoride removal. Therefore, we can conclude that electrostatic interaction was also involved in the adsorption of fluoride. This result was in agreement with the effect of pH discussed above.

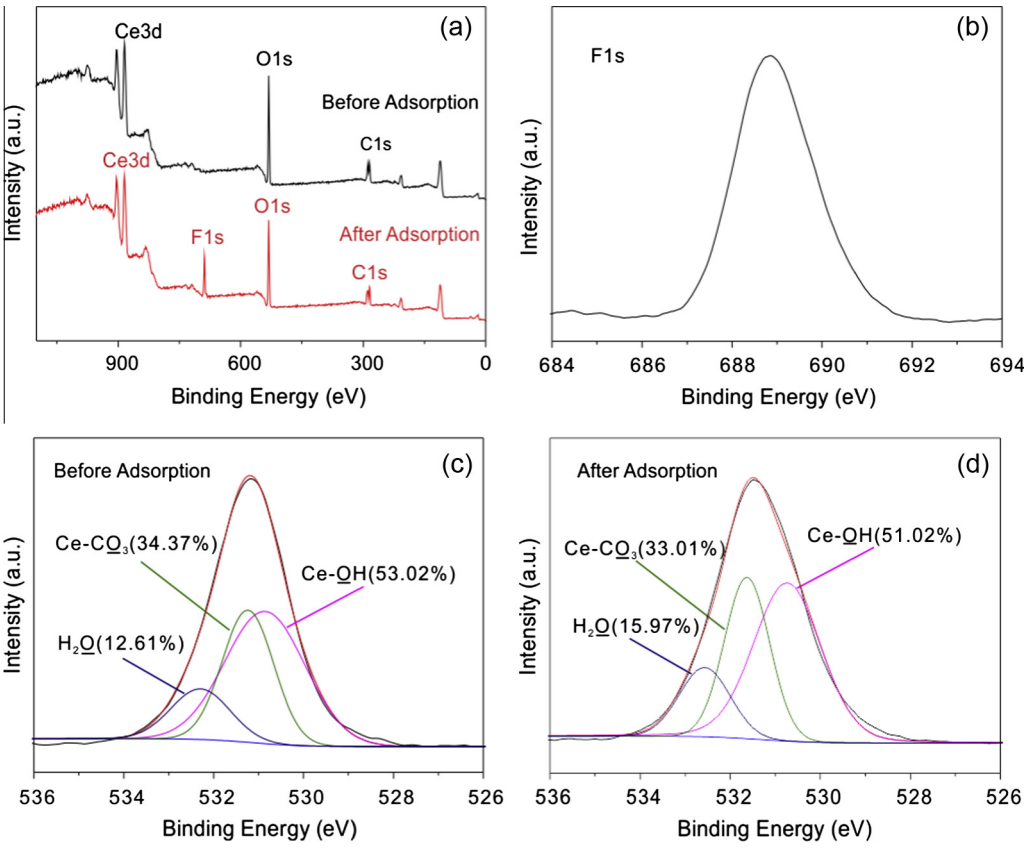

Fig. 10. XPS survey spectra (a) of the obtained $CeCO_3OH$ nanospheres before and after fluoride removal. F1s spectrum (b) of $CeCO_3OH$ nanospheres after fluoride adsorption. O1s spectra of the obtained $CeCO_3OH$ nanospheres before (c) and after (d) fluoride removal.

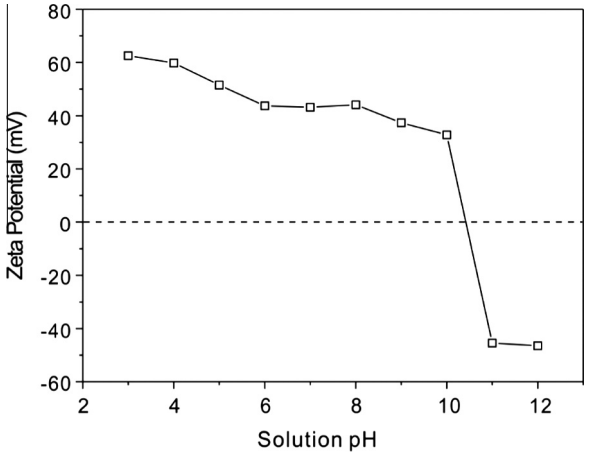

Fig. 11. Zeta potential of the$CeCO_3OH$ nanospheres at different pH values.

4. Conclusions

In summary, we have described a one-step approach to $CeCO_3OH$ nanospheres with uniform size, and demonstrate that the $CeCO_3OH$ nanospheres show excellent fluoride removal performance due to electrostatic interaction and exchange of the carbonate and hydroxyl groups on the adsorbent surface with fluoride anions according to EDS, FT-IR, XPS and zeta potential analysis. In addition, adsorption kinetics fit well the pseudo-second-order model and the adsorption isotherm could be described very well by the Langmuir model. The adsorption efficiency even reaches up to 93.0%, 96.8% and 91.0% at pH = 7 ± 0.2 for initial low fluoride concentrations of 10, 20 and 30 mg/L, respectively. Moreover, this adsorbent possesses a considerable wide pH range (3–10) and has less influence on adsorption of F^- by co-exiting ions. This research results indicate that the fluoride removal ratio is very high at the low initial fluoride concentrations in the basis of the equilibrium adsorption capacities and the adsorbent could be a potentially suitable material used in the fluoride removal.

Acknowledgements

The authors gratefully acknowledge financial support from the National Key Scientific Program-Nanoscience and Nanotechnology (Grant No. 2011CB933700) and the National Natural Science Foundation of China (21277146, 61374017, 1205204, 21177131, 61273066, and 61104205).

Appendix A. Supplementary material

Supplementary data associated with this article can be found, in the online version, at http://dx.doi.org/10.1016/j.jcis.2016.04.037.

References

[1] World Health Organization, Guidelines for Drinking-Water Quality: Incorporating First Addendum Recommendations, 1, third ed., World Health Organization, 20 Avenue Appia, 1211 Geneva 27, Switzerland, 2006, pp. 375–376.
[2] S. Jagtap, M.K. Yenkie, N. Labhsetwar, S. Rayalus, Fluoride in drinking water and defluoridation of water, Chem. Rev. 112 (4) (2012) 2454–2466.
[3] F.L. Theiss, S.J. Couperthwaite, G.A. Ayoko, R.L. Frost, A review of the removal of anions and oxyanions of the halogen elements from aqueous solution by layered double hydroxides, J. Colloid Interf. Sci. 417 (2014) 356–368.

[4] P. Loganathan, S. Vigneswaran, J. Kandasamy, R. Naidu, Defluoridation of drinking water using adsorption processes, J. Hazard. Mater. 248 (2013) 1–19.
[5] X.L. Yu, S.R. Tong, M.F. Ge, J.C. Zuo, Removal of fluoride from drinking water by cellulose@hydroxyapatite nanocomposites, Carbohyd. Polym. 92 (1) (2013) 269–275.
[6] N.D. Ravi, R. Balu, T.S.S. Kumar, Strontium-substituted calcium deficient hydroxyapatite nanoparticles: synthesis, characterization, and antibacterial properties, J. Am. Ceram. Soc. 95 (9) (2012) 2700–2708.
[7] D.Y. Zhang, H.M. Luo, L.W. Zheng, K.J. Wang, H.X. Li, Y. Wang, H.X. Feng, Utilization of waste phosphogypsum to prepare hydroxyapatite nanoparticles and its application towards removal of fluoride from aqueous solution, J. Hazard. Mater. 241 (2012) 418–426.
[8] S. George, P. Pandit, A.B. Gupta, Residual aluminium in water defluoridated using activated alumina adsorption – modeling and simulation studies, Water Res. 44 (10) (2010) 3055–3064.
[9] S.S. Tripathy, A.M. Raichur, Abatement of fluoride from water using manganese dioxide-coated activated alumina, J. Hazard. Mater. 153 (3) (2008) 1043–1051.
[10] V.S. Chauhan, P.K. Dwivedi, L. Iyengar, Investigations on activated alumina based domestic defluoridation units, J. Hazard. Mater. 139 (1) (2007) 103–107.
[11] M.S. Onyango, T.Y. Leswifi, A. Ochieng, D. Kuchar, F.O. Otieno, H. Matsuda, Breakthrough analysis for water defluoridation using surface-tailored zeolite in a fixed bed column, Ind. Eng. Chem. Res. 48 (2) (2009) 931–937.
[12] M.S. Onyango, Y. Kojima, O. Aoyi, E.C. Bernardo, H. Matsuda, Adsorption equilibrium modeling and solution chemistry dependence of fluoride removal from water by trivalent-cation-exchanged zeolite F-9, J. Colloid Interf. Sci. 279 (2) (2004) 341–350.
[13] S. Meenakshi, N. Viswanathan, Identification of selective ion-exchange resin for fluoride sorption, J. Colloid Interf. Sci. 308 (2) (2007) 438–450.
[14] N. Viswanathan, S. Meenakshi, Role of metal ion incorporation in ion exchange resin on the selectivity of fluoride, J. Hazard. Mater. 162 (2–3) (2009) 920–930.
[15] W.Y. Li, J. Liu, H. Chen, Y. Deng, B. Zhang, Z. Wang, X. Zhang, S. Hong, Application of oxalic acid cross-linking activated alumina/chitosan biocomposites in defluoridation from aqueous solution. Investigation of adsorption mechanism, Chem. Eng. J. 225 (2013) 865–872.
[16] B. Xu, Q.T. Zhang, S.S. Yuan, M. Zhang, T. Ohno, Morphology control and photocatalytic characterization of yttrium-doped hedgehog-like CeO_2, Appl. Catal. B – Environ. 164 (2015) 120–127.
[17] F. Yang, J.J. Wei, W. Liu, J.X. Guo, Y.Z. Yang, Copper doped ceria nanospheres: surface defects promoted catalytic activity and a versatile approach, J. Mater. Chem. A 2 (16) (2014) 5662–5667.
[18] X.Y. Wu, H.L. Niu, S.S. Fu, J.M. Song, C.J. Mao, S.Y. Zhang, D.W. Zhang, C.L. Chen, Core-shell CeO_2@C nanospheres as enhanced anode materials for lithium ion batteries, J. Mater. Chem. A 2 (19) (2014) 6790–6795.
[19] N. Viswanathan, S. Meenakshi, Enhanced fluoride sorption using La(III) incorporated carboxylated chitosan beads, J. Colloid Interf. Sci. 322 (2) (2008) 375–383.
[20] H. Liu, S.B. Deng, Z.J. Li, G. Yu, J. Huang, Preparation of Al-Ce hybrid adsorbent and its application for defluoridation of drinking water, J. Hazard. Mater. 179 (1–3) (2010) 424–430.
[21] S.B. Deng, H. Liu, W. Zhou, J. Huang, G. Yu, Mn-Ce oxide as a high-capacity adsorbent for fluoride removal from water, J. Hazard. Mater. 186 (2–3) (2011) 1360–1366.
[22] J. Wang, W. Xu, L. Chen, Y. Jia, L. Wang, X.-J. Huang, J. Liu, Excellent fluoride removal performance by CeO_2–ZrO_2 nanocages in water environment, Chem. Eng. J. 231 (2013) 198–205.
[23] C.Y. Cao, P. Li, J. Qu, Z.F. Dou, W.S. Yan, J.F. Zhu, Z.Y. Wu, W.G. Song, High adsorption capacity and the key role of carbonate groups for heavy metal ion removal by basic aluminum carbonate porous nanospheres, J. Mater. Chem. 22 (37) (2012) 19898–19903.
[24] L. Chang, F.X. Wang, D. Xie, J. Zhang, G.H. Du, Graphite oxide-mediated synthesis of porous CeO_2 quadrangular prisms and their high-efficiency adsorptive performance, Mater. Res. Bull. 48 (10) (2013) 4362–4367.
[25] Y. Yin, A.P. Alivisatos, Colloidal nanocrystal synthesis and the organic-inorganic interface, Nature 437 (7059) (2005) 664–670.
[26] Z.Y. Guo, F.L. Du, Z.L. Cui, Hydrothermal synthesis of single-crystalline $CeCO_3OH$ flower-like nanostructures and their thermal conversion to CeO_2, Mater. Chem. Phys. 113 (1) (2009) 53–56.
[27] K.S. Zhang, S.B. Wu, X.L. Wang, J.Y. He, B. Sun, Y. Jia, T. Luo, F.L. Meng, Z. Jin, D.Y. Lin, W. Shen, L.T. Kong, J.H. Liu, Wide pH range for fluoride removal from water by MHS-MgO/$MgCO_3$ adsorbent: kinetic, thermodynamic and mechanism studies, J. Colloid Interf. Sci. 446 (2015) 194–202.
[28] Y.S. Ho, G. McKay, Pseudo-second order model for sorption processes, Process Biochem. 34 (5) (1999) 451–465.
[29] T.W. Weber, R.K. Chakravorti, Pore and solid diffusion models for fixed-bed adsorbers, Aiche J. 20 (2) (1974) 228–238.
[30] H. Freundlich, Over the adsorption in solution, J. Phys. Chem. 57 (385) (1906) e470.
[31] X.D. Zhao, D.H. Liu, H.L. Huang, W.J. Zhang, Q.Y. Yang, C.L. Zhong, The stability and defluoridation performance of MOFs in fluoride solutions, Micropor. Mesopor. Mater. 185 (2014) 72–78.
[32] D. Dayananda, V.R. Sarva, S.V. Prasad, J. Arunachalam, N.N. Ghosh, Preparation of CaO loaded mesoporous Al_2O_3: efficient adsorbent for fluoride removal from water, Chem. Eng. J. 248 (2014) 430–439.
[33] T. Zhang, Q.R. Li, H.Y. Xiao, Z.Y. Mei, H.X. Lu, Y.M. Zhou, Enhanced fluoride removal from water by non-thermal plasma modified CeO_2/Mg–Fe layered double hydroxides, Appl. Clay Sci. 72 (2013) 117–123.
[34] M.G. Sujana, A. Mishra, B.C. Acharya, Hydrous ferric oxide doped alginate beads for fluoride removal: adsorption kinetics and equilibrium studies, Appl. Surf. Sci. 270 (2013) 767–776.
[35] Y.H. Li, Q.J. Du, J.J. Wang, T.H. Liu, J.K. Sun, Y.H. Wang, Z.H. Wang, Y.Z. Xia, L.H. Xia, Defluoridation from aqueous solution by manganese oxide coated graphene oxide, J. Fluorine Chem. 148 (2013) 67–73.
[36] Y.L. Nie, C. Hu, C.P. Kong, Enhanced fluoride adsorption using Al (III) modified calcium hydroxyapatite, J. Hazard. Mater. 233 (2012) 194–199.
[37] B. Zhao, Y. Zhang, X.M. Dou, X.M. Wu, M. Yang, Granulation of Fe-Al-Ce trimetal hydroxide as a fluoride adsorbent using the extrusion method, Chem. Eng. J. 185 (2012) 211–218.
[38] S.L. Gai, P.P. Yang, X.B. Li, C.X. Li, D. Wang, Y.L. Dai, J. Lin, Monodisperse CeF_3, CeF_3:Tb^{3+}, and CeF_3:Tb^{3+}@LaF_3 core/shell nanocrystals: synthesis and luminescent properties, J. Mater. Chem. 21 (38) (2011) 14610–14615.
[39] Y. Zhai, S. Zhang, H. Pang, Preparation, characterization and photocatalytic activity of CeO_2 nanocrystalline using ammonium bicarbonate as precipitant, Mater. Lett. 61 (8–9) (2007) 1863–1866.
[40] G.S. Li, S.H. Feng, L.P. Li, Structural stability and valence characteristics in cerium hydrothermal systems, J. Solid State Chem. 126 (1) (1996) 74–79.
[41] S.F. Wang, F. Gu, C.Z. Li, H.M. Cao, Shape-controlled synthesis of $CeOHCO_3$ and CeO_2 microstructures, J. Cryst Growth 307 (2) (2007) 386–394.
[42] K.Y. Li, F.F. Chai, Y.Q. Zhao, X.W. Guo, Facile synthesis of magnetic Fe_3O_4/$CeCO_3OH$ composites with excellent adsorption capability for small cationic dyes, RSC Adv. 5 (114) (2015) 94397–94404.